https://dx.doi.org/10.1016/j.conbuildmat.2023.133084

Micropore Structure Characterization of the Bitumen Emulsion-based Cold In-place Recycling Mixture Considering Water Gradient Migration Condition through Multiple XCT Scanning

Zili Zhao[1], Jiwang Jiang[1, *], Zhen Leng[2, *], Fujian Ni[1]

[1] College of Transportation Engineering, Southeast University, Nanjing, Jiangsu, China, 211189

[2] Department of Civil and Environmental Engineering, the Hong Kong Polytechnic University, Kowloon 999077, Hong Kong

[*] Corresponding author. Email: jiang_jiwang@seu.edu.cn (J. Jiang), zhen.leng@polyu.edu.hk(Z. Leng)

Abstract

Bitumen Emulsion-based Cold In-place Recycling (BE-CIR) has been widely used all around the world due to its superior environmental benefits. Unlike the hot mix asphalt (HMA), BE-CIR mixture presents a unique moisture migration behavior after compaction. The migration of water can alter the micro-pore structure of the BE-CIR mixture and then change its mechanical performance. Therefore, it is essential to characterize the variation of internal structure, especially the air voids, in depth direction during the curing process of BE-CIR mixture. A one-way evaporation method was developed to simulate the field moisture migration of BE-CIR mixture specimens in laboratory. To track the internal structure change with time, multiple X-ray Computed Tomography (XCT) scanning examinations were performed on the lab-prepared specimens with three different curing periods (0h, 60h, and 153h). The effects of curing temperature and initial moisture content on the micropore structure development were also investigated. The morphology variations of air voids including the content, number, volume distribution and void gradation in the depth direction with curing time were further characterized. The results indicate that there is a 0.5% difference in air void content between the top and bottom of the BE-CIR mixture. The BE-CIR mixture's micropore structure evolved over the course of curing with two key characteristics: a fast increase in the number of small voids and a sustained development of large voids. The development of more tiny pores and the gradient properties of these pores, which predominated during the curing time of 60 to 153h, were a reflection of the internal migration of free water. The initial moisture content mainly affects the magnitude of the large void variation during the curing time of 0 to 60h, while the curing temperature affects the proportion of pore increase between the two curing periods. The outcomes can provide a better understanding on the dynamic volumetric characteristics of the BE-CIR pavement over the curing process.

Keywords: bitumen emulsion, cold-in-place recycling, moisture migration, XCT scanning, image analysis, micropore structure.

1 Introduction

Depletion of natural resource necessitates the adoption of recycling as a rehabilitation technology in pavement engineering. Reclaimed asphalt pavement (RAP) material is obtained by milling distressed pavements or from full depth removal of asphalt pavements. Of the different technologies that exist, the Cold In-place Recycling (CIR) pavement is a green technique that enables 100% reuse in the process of recycling asphalt pavements without the need for heating and transportation[1, 2]. In recent years, it has gained worldwide popularity as a cost-effective and environment-friendly pavement rehabilitation strategy in many countries, such as USA, Canada, Spain, Greece, Germany, China, and India [3, 4]. Many attractive features are also available, including the ability to completely repair pavement defects such as potholes, rutting, irregular cracks, and reflection cracks, as well as extending the life of asphalt pavements, reducing landfill disposal pressure and improving ride comfort [5]. The lower working temperature is achieved by using bitumen emulsion or foam as binder used in CIR, which presents significantly lower viscosities than traditional bitumen, thereby allowing the mixing and compaction operations to be done at room temperatures. Apart from the bitumen, some inorganic Additives, such as Portland cement are frequently used to facilitate dispersion of bitumen, regulate the breaking of the emulsion, accelerate the curing time, and improve the mechanical properties of the CIR mixture [6, 7]. Generally speaking, the CIR technology is more commonly used in base course due to the inferior mechanical performance. The viscosity reduction mechanism for foamed and emulsified bitumen are different. Both techniques have been used widely for the cold recycling of pavement. For this research, it mainly focused on the Bitumen Emulsion-based Cold In-place Recycling (BE-CIR) technology. Moreover, the moisture characterization methods used for BE-CIR mixture should be also suitable for the foamed one, because both techniques add water to the system for mixing and compaction [8, 9].

In order to promote the uniform coating of the bitumen emulsion and enhance the packing of RAP aggregates, a certain amount of water is usually added during the mixing process, depending on the field environmental conditions[10, 11]. Upon compaction, curing process accompanied by water-related phenomena, such as seepage, evaporation, suction, emulsion breaking, and cement hydration, normally lead to a reduction of moisture and an increase in stiffness and strength[12-14]. The development of the curing process is affected by material-related factors such as dosage of bituminous and cementitious binders, initial moisture content, etc., construction-related factors

of drainage conditions, layer thickness, and compaction level and environmental-related factors of temperature, humidity, wind, and rain [15-19]. It is challenging to simulate the potential evolution of material properties of BE-CIR mixture in the field since environmental-related variables are so unpredictable.

Many lab-curing protocols with specific temperature and relative humidity conditions were documented for the fabrication of BE-CIR mixtures in laboratory. The surface treatment methods of the compacted specimens usually have two types: unsealed (free evaporation) and sealed (wrapped in a plastic bag). These protocols usually accelerate the curing process and the cured specimens would be used to characterize or rank the performance of different BE-CIR mixtures [20-22]. Under field circumstances, the accelerated curing process can barely simulate the in-suit curing condition, and consequently specimens subjected to accelerated curing process can hardly be used to accurately predict the short and long-term field performance[23, 24]. Researchers have installed moisture sensors and temperature sensors in the CIR pavement to measure water content and temperature of the BE-CIR mixtures over curing process[23, 25-27]. In order to recommend the timing of HMA overlay or validate the laboratory curing protocols under local humidity and temperature conditions, some researchers have evaluated the fluctuation of moisture during compaction[26] and the short-term[25] or long-term[23] curing process.

In most cases, the BE-CIR layer is viewed as an integrated whole when measuring moisture migration, and moisture fluctuation in the depth direction during curing is ignored. To address this problem, Zhao et al. [8] monitored the in-situ moisture condition of BE-CIR pavement at different depths by humidity and temperature sensors and they found that the in-situ moisture migration of BE-CIR pavement presents a unique gradient characteristics. With the evaporation of water, the air voids in BE-CIR field cores also present a gradient feature from the top to bottom. It is believed that air void is an important factor affecting the performance of BE-CIR mixtures. The designed air void content for BE-CIR mixture is between 8% and 15% and changes during the curing process with the loss the water[28]. Unlike HMA, due to the gradient moisture migration, one single air void content can hardly reflect the pore-structure of BE-CIR mixture. The X-ray CT scanning test is considered to be an efficient method to quantify the internal structure of mixture. Although this method is common for HMA [29, 30], very little work has been carried out on CIR. Gao et al.[31] conducted a tomography study on BE-CIR mixture and found that the air void distribution was different for three different compaction methods (Marshall, static, and gyratory compaction) and

had a significant difference with HMA. Nivedya et al.[32] quantified the air void distribution of CIR with different designed cement and air void content using X-ray CT test. Even-through these researches have reported the air void distribution of BE-CIR mixture using image analysis and XCT scanning method, the evolution law of the micropore structure of BE-CIR mixture over curing process is still unclear. Also, it is important to reveal the effect of gradient moisture migration on the development of micropore structure, which may shed more lights on the microstructure of BE-CIR pavement.

2 Objectives and Scopes

This study employed a semi-sealed laboratory curing condition (specimen with waterproofing layer covered around the side and bottom surface) to simulate the field moisture migration. Multiple XCT scanning tests were used to characterize the micropore structure of BE-CIR mixture at different curing times. The objectives are to 1) investigate the development of air void content and void morphology of BE-CIR mixture with curing times; 2) characterize the development of micropore structure characteristic in depth direction of the BE-CIR specimen; and 3) explore the effects of curing temperature and initial moisture content on the evolution law of micropore in BE-CIR mixture.

3 Mix Design and Fabrication

3.1 Materials and mixture design

The RAP materials used in this study were collected from a pavement maintenance project using BE-CIR technology of Fenguan Highway (G15) in Lianyungang, Jiangsu Province of China in May, 2022. The materials and mixture design were consistent with the project[8]. One cationic slow-setting emulsified bitumen and one ordinary Portland cement (PO. 42.5) were collected from the project for the fabrication of BE-CIR mixture. The basic properties of the emulsified bitumen are described in Table 1 according to the Chinese Specifications “Standard Test Methods of Bitumen and Bituminous Mixtures for Highway Engineering”[33]. As demonstrated in Figure 1, the gradation of BE-CIR mixture fell within the medium gradation limitations specified by Jiangsu Province agency [34].

In our project, the structure design for this project was to regenerate the original 10 cm surface layer into an entire BE-CIR layer, followed by a 5 cm overlay layer on top of it. In order to solve

the problems of the lack of high temperature performance and the weak early strength, a relatively high cement content of 2.2 wt% was determined. The optimum asphalt emulsion content was determined to be 3.3 wt% with satisfactory Marshal Stability and Indirect Tensile Strength. The optimal total moisture content was determined to be 4.0 wt% using the maximum dry density method (MOT, 2019) and the extra water was 2.8 wt% by subtracting the water in emulsified bitumen.

Table 1 Properties of emulsified bitumen

Characteristics of the emulsified bitumen	
Residue content by evaporation (%)	64
Penetration (25 ℃; 0.1 mm)	59.1
Softening point (◦C)	59.9
Ductility (15 ℃; cm)	110
Sieve residue (1.18 mm; %)	0.03
Storage stability (5 d, 25℃; %)	1.47
Storage stability (1 d, 25℃; %)	0.42

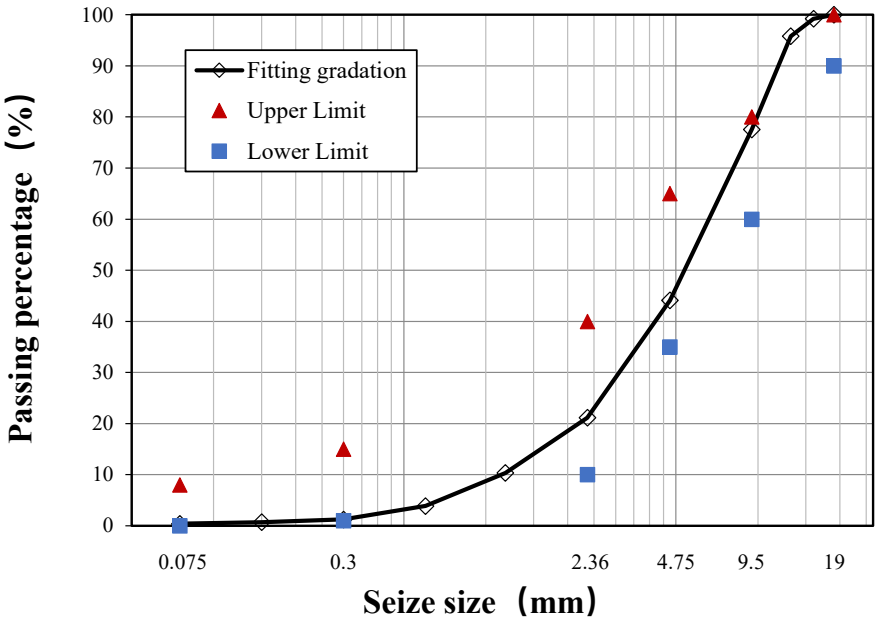

Figure 1 Aggregate gradation of BE-CIR mixtures.

3.2 Compaction and curing condition

The Superpave gyratory compaction (SGC) method was utilized to prepare BE-CIR mixture. Specimens with a diameter of 100 mm and a height of 100 mm were prepared. The BE-CIR

mixtures were produced by initially adding the cement to the RAP and mixing with extra water for one minute, then the emulsified bitumen was added and mixed for another four minutes. The gyratory number was set as 30 for all specimens to ensure that the compaction energy of all samples was the same. The number of gyratory gyrations for the compaction was determined to achieve the target air void of 10% which was consisted with the mix design of the in-situ BE-CIR project[8].

The compacted BE-CIR specimens usually were cured in the oven unsealed at a specified constant temperature. This curing method was widely used due to its simplicity and time-saving[20, 21]. However, it considers the BE-CIR specimen as an integrated whole but ignores the gradient moisture migration characteristics under the boundary condition in the field environment. Therefore, a semi-sealed laboratory curing condition was designed to simulate the in-situ moisture migration process. A waterproofing layer was covered around the side and bottom surface of the specimens (Figure 2) to ensure moisture inside the mixture can only evaporate from the upper surface.

Two important factors affecting water evaporation are considered in this paper, which are the initial moisture content and the constant curing temperature. As shown in Table 2, BE-CIR1 represents the initial moisture content of 4%, and the curing temperature was 40℃ to simulate the construction of BE-CIR in summer base on the field project data from the previous study[8]. BE-CIR2 has a higher initial moisture content of 4.5% than BE-CIR 1, while BE-CIR 3 has a lower curing temperature of 25℃. Three parallel specimens oof each BE-CIR were fabricated for the following test.

Table 2 Controlled variable of different mixture

	Initial moisture content (%)	Curing temperature (℃)
BE-CIR1	4.0	40
BE-CIR2	4.5	40
BE-CIR3	4.0	25

4 Experimental Program

4.1 Multiple XCT scanning test

Figure 2 illustrates the overall process of the test. Since the XCT scan cost about 2-3 hours of each specimen, each specimen was compacted every 3 hours to ensure the same curing time when it

was scanned. After compaction, CT scan was performed immediately and the results was recorded as 0h. Then, the sample was placed in the oven at the corresponding constant temperature for curing. According to a previous study about the moisture migration of BE-CIR in the field based on humidity sensors, the change of moisture content during curing in the field presents two obvious stages[8]. In that study, the sensor output was defined as humidity index (HI) which could qualitatively indicate the moisture content. The first stage is the HI drops rapidly lasting approximately 3 days, and in the second stage, HI decreases slowly and becomes stable with the increased curing time. Moreover, the overlay of BE-CIR pavement usually was paved after 7 days of curing, by which time most of the moisture had evaporated. Therefore, curing time of 60h (almost 3 days) and 153h (almost 7 days) was chosen for testing in this paper. In each testing time, the mass of each sample was recorded firstly, and then XCT scan was conducted. A total of 3 times of XCT scanning were conducted for each specimen at the curing times of 0h, 60h and153h, respectively.

The XCT scanning test was conducted by a computed tomography equipment model phoenix v|tome|x. A voltage of 140kV was hence applied with an electric current of 72μA, so it can emit more dense X-rays and obtain images based on high-frequency algorithms. The spatial resolution was set as 60.1μm. In this case, 1832 two dimensional cross-sections (slices of 1747 pixels x 1747 pixels) could be achieved from each sample.

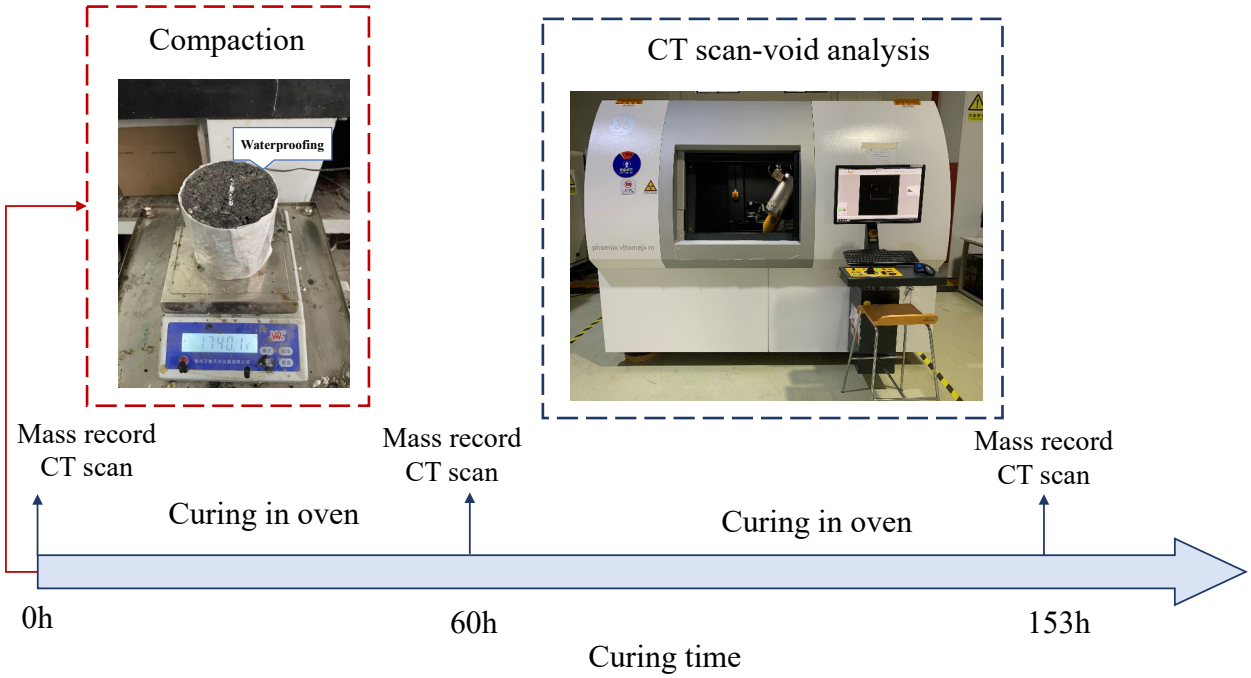

Figure 2 Overall process of experiment

4.2 Void parameter based on CT scanning test

4.2.1 Voids identification from 3D reconstruction

The reconstruction of the three-dimensional microstructures of BE-CIR specimens was accomplished with the software Avizo. In order to eliminate the edge effect, the middle 1700 slices were selected for 3D reconstruction. In the cross-section CT image as shown in Figure 3, the mixture entity with different gray levels could be easily identified, and the voids were black inside the mixture. According to the principle of CT scan, the different grey levels of materials depended on their density. It is known that the density of aggregate is around 2.5 to 3 g/cm^3 which is largest in this system, and therefore has the brightest color in the image. The rest part with gray levels was the bitumen-cement mortar whose density range between 1 to 2 g/cm^3. As the density of bitumen is around 1.03 g/cm^3, while the density of water is 1 g/cm^3 which is extremely close to the binder, it is hardly to distinguish water separately from the mortar. Therefore, the moisture was considered as part of the mixture in this study. Based on this, at each curing time, the identified void was not the true size void of this sample, but the void after the removal of water.

By distinguishing the grayscale of the 3D model, voids with a volume greater than 2.17E-4 mm^3 were detected. As shown in Figure 4, the image parameters were converted to the coordinates in

the 3D model, based on this, the location which is the centroid coordinates of each void was obtained and the volume of each void were calculated. Furthermore, in order to study the distribution of voids in the thickness direction, 10 different regions every 1cm along the thickness direction of each specimen were analyzed. Three-dimensional reconstruction was carried out on these regions respectively (170 two dimensional cross-sections) to calculate the volume parameter same as the overall specimen. In this paper, 11 three-dimensional microstructures model were reconstructed of each CT scan results, thus a total of 99 microstructures models were calculated.

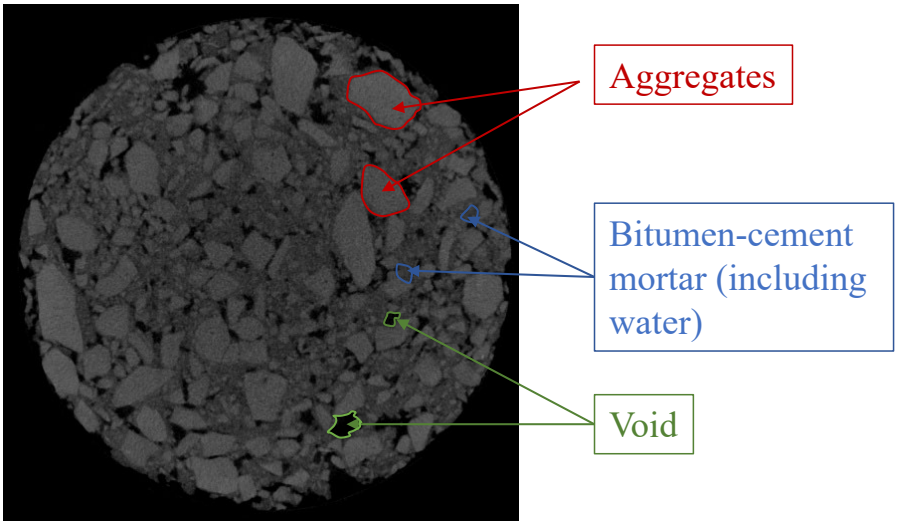

Figure 3 Different components in a cross-section image.

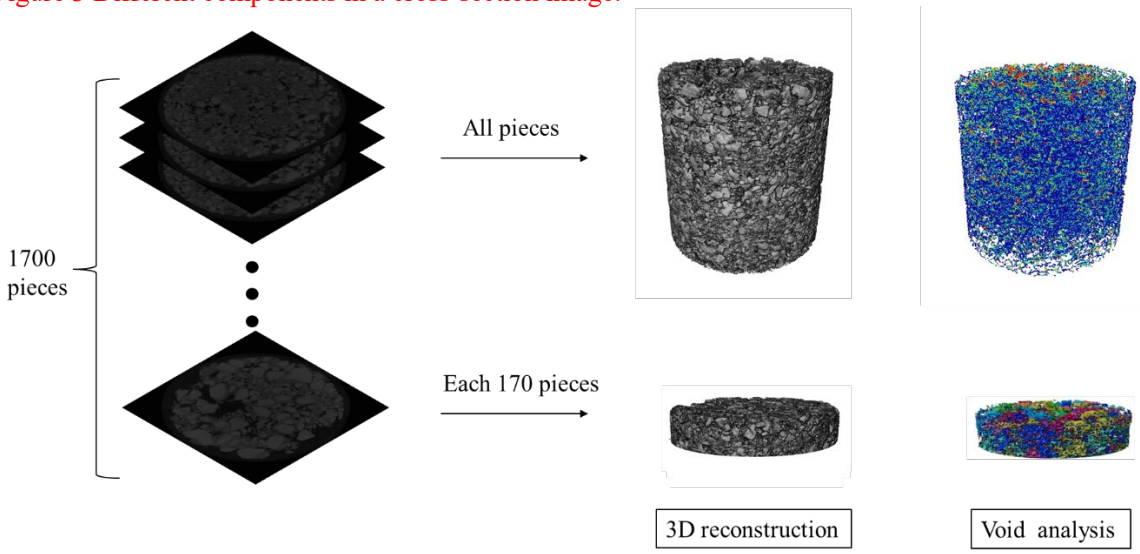

Figure 4 Three-dimensional reconstruction and void analysis

4.2.2 Calculation of void gradation

For the purpose of an advanced study of the statistical properties of voids, the concept of void grading is introduced. Similar to the aggregate gradation, voids are filtered according to their equivalent diameter by setting a series of sieve size. The equivalent diameter is calculated by treating each void as a sphere and using its volume to calculate the equivalent diameter, so the units in the void gradation is mm. It is important to note that for the aggregate gradation, the passing percentage is calculated by mass, while here for voids the passing percentage is calculated by volume assuming that the density of the gas in all voids is the same. Hence the passing percentage of a given sieve size is actually the volume proportion of all voids with an equivalent diameter smaller than the sieve size. For ease of understanding, the same sieve size as the aggregate gradation is used, but a 6.7 sieve is added between 4.75 and 9.5 mm to smooth out the gradation curve. Figure 5 shows the void gradation of BE-CIR1 at 0h as an example. A similar morphology can be found in the void gradation and aggregate gradation curves. It is somewhat analogous to intermittent grading, with a rapid decrease in the passing percentage of sieve size from 9.5mm to 2.36mm. The maximum void equivalent diameter is smaller than 13.2mm.

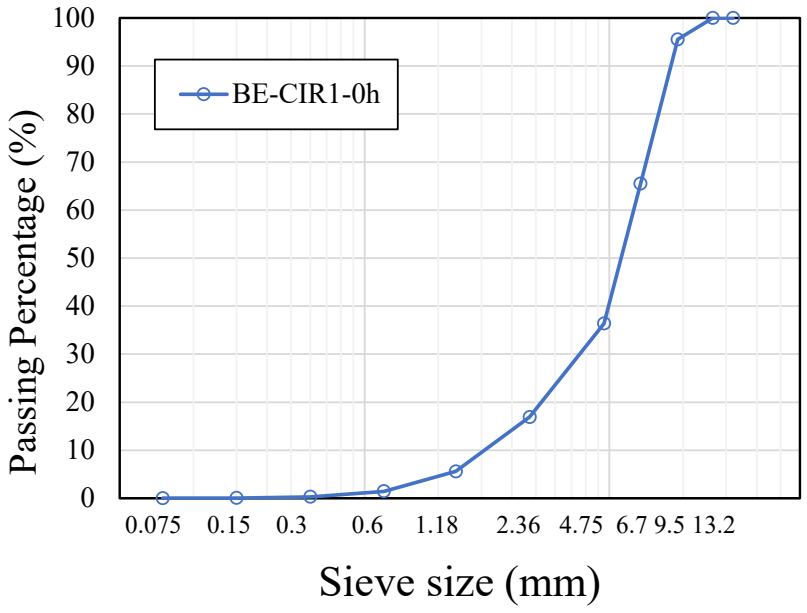

Figure 5 Typical void gradation of BE-CIR

5 Discussion of Results

5.1 Weight loss

The weight loss is defined by Eq. (1), and Figure 6 illustrates the weight loss during curing time. The two time periods 0-60h and 60-153h have significantly different rates of change in weight loss. In curing time of 0-60h, the weight loss increased rapidly due to a greater moisture content and faster water evaporation. After curing for 60 h, the weight loss gradually stabilized. Comparing different BE-CIR mixture, BE-CIR2 showed a greater weight loss due to the higher initial moisture content than the other two. The cumulative weight loss of BE-CIR3 was significantly smaller than BE-CIR1, while the difference between BE-CIR1 and BE-CIR2 was very little. Thus, in view of the water losses during the curing, the influence of 15 °C curing temperature difference was greater than that of 0.5% initial moisture content.

$$\text{Weight loss} = (m_i - m_0)/m_0 \quad (1)$$

where m_i represents the mass of specimen at curing time of i hour (g), and m_0 is the mass of the specimen at 0h (g).

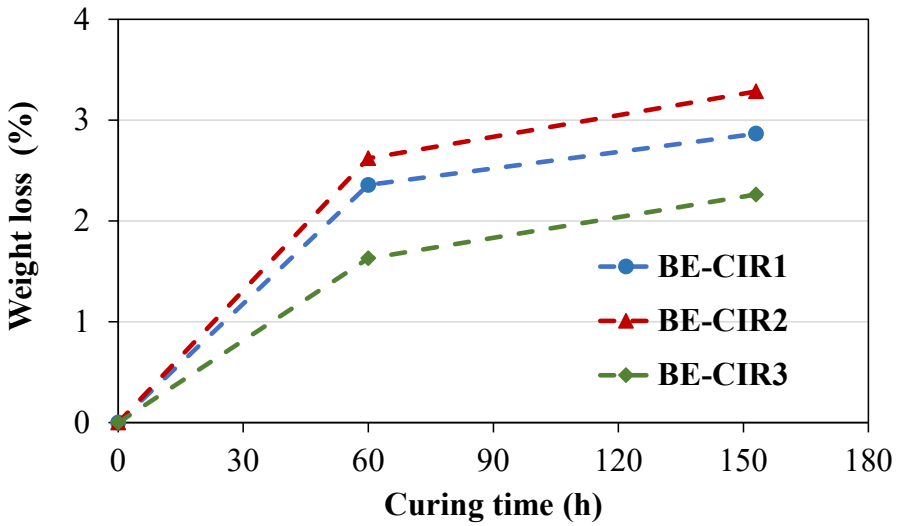

Figure 6 Variation of weight loss over curing time

5.2 Air void content

During the curing process of BE-CIR mixture, the variation of air void may be influenced by compact (which would happen under traffic in the field), the evaporation and migration of water

and the hydration of the cement. Since in this study the specimens were not subjected to compact during the curing, the change in air void due to rotational of the aggregates was not considered. According to the Section 4.2.1, the variation in air void in this paper is mainly due to the dissipation of water in the void. It is difficult to indicate precisely whether this part of the water evaporated or hydrated from this method. However, on the one hand the water that can be absorbed by cement is generally about 1/3 of the cement content, which in this paper means that 1/3 of cement content 2.2% is 0.7%. The initial moisture content of the mix is 4%, which means that the additional water of 3.3% needs to be dissipated by evaporation. On the other hand, the cement particles could wrap in some water during the compaction, this part of water undergoes hydration reaction with cement, and produce some micro-pores. The micro voids in cement hydration products are generally a few tens of nanometers in size, with the larger voids being only a few microns in size, which are much smaller than the accuracy of the XCT scanning method in this paper. Therefore, it can be approximated that the variation in air voids in this study is mainly due to water evaporation.

Figure 7 shows the variation of the overall air void content (AV) with the curing time. Obviously, with the increase of curing time, the AV of each BE-CIR increased continuously caused by the evaporation of water inside the mixture. Among three different BE-CIRs, BE-CIR2 had the largest original air void content (6.6% at curing time 0h). This may due to the negative effect of the high initial moisture content during compaction. Considering the increasement of air void content during curing, the trend of BE-CIR1 and BE-CIR3 was consistent with the weight loss. Since BE-CIR1 has higher curing temperature than BE-CIR3, it had a greater mass loss, resulting in higher air void content. Meanwhile, similar to weight loss, the growth of air void content of BE-CIR1 between 0h-60h was larger than that of BE-CIR3, while it was smaller between 60h-153h.

It should be noted that the so-called air void content was calculated by the void with water removed, so the air void at 0h appeared relatively small. In addition, the curing method used in determining the number of gyrations is an accelerated curing method, i.e. specimens was unsealed and cured in oven at 60°C for 48 hours[34]. In that situation, the water inside the mixture could evaporate almost completely, while the semi-sealed laboratory curing condition used in this paper may result in incomplete evaporation of water, so that the air void of three BE-CIR at 153h was smaller than the target air void of 10%.

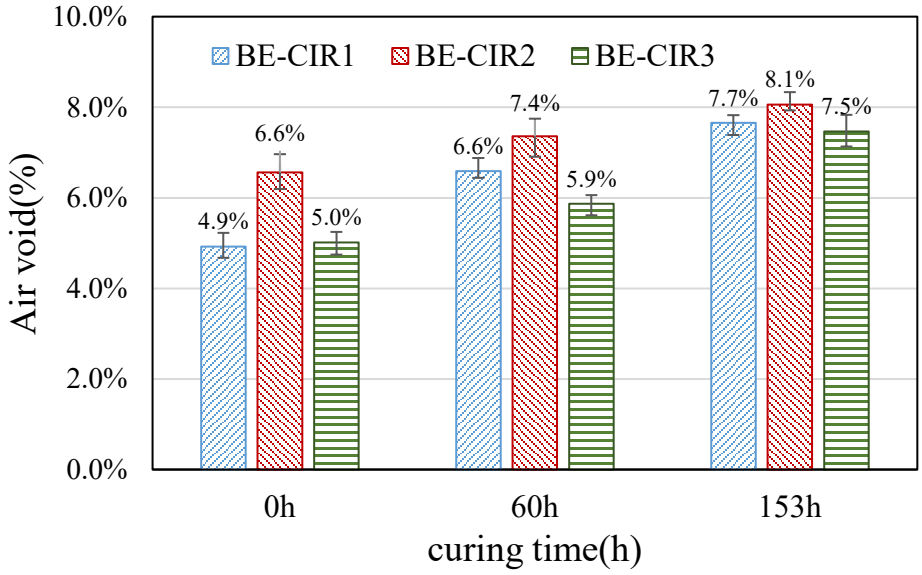

Figure 7 Variation of overall air void content

5.3 Development of voids with different volumes

5.3.1 Void number distribution

According to the reconstruction of the three-dimensional microstructures, total void number and volume was calculated as presented in Figure 8. The blue, green, red color in Figure 8 represents voids with volume less than 1 mm^3, 1 to 10 mm^3 and bigger than 100 mm^3 respectively. It can be found that both total void number and volume of each CIR increased with the curing time. In addition, the distribution of numbers of voids for different volumes was analyzed based on the volume of each void. As shown in Figure 9 (a)(c)(e), number of voids with the volume smaller than 1mm^3 was the majority in the distribution. Consider the change of void number over curing time, the increasement of void number only occurred in voids with the volume less than 1 mm^3 and bigger than 200 mm^3. At the same time, the void volume between 0 and 0.01 mm^3 has the largest increase in the number of voids. This can be concluded that the increase of the total void number is mainly due to the increase of small volume voids. In addition, theoretically speaking, the increase in the void number is mainly due to the evaporation of water in the process of curing, while the significant increase in the number of small voids indicates that water mainly exists in the form of capillary water.

Comparing three different CIR, BE-CIR1 and BE-CIR3 showed a consistent trend in the number of voids over curing time, while for BE-CIR2, the increment of void with the volume less than

306 0.01 mm3 between 60 and 153 hours was significantly larger than that between 0 and 60 hours. It
307 indicates that in the case of more initial water content, the void development in the early stage of
308 curing is mainly the evaporation of residual water in the larger voids, while the evaporation time
309 of capillary water is relatively later.

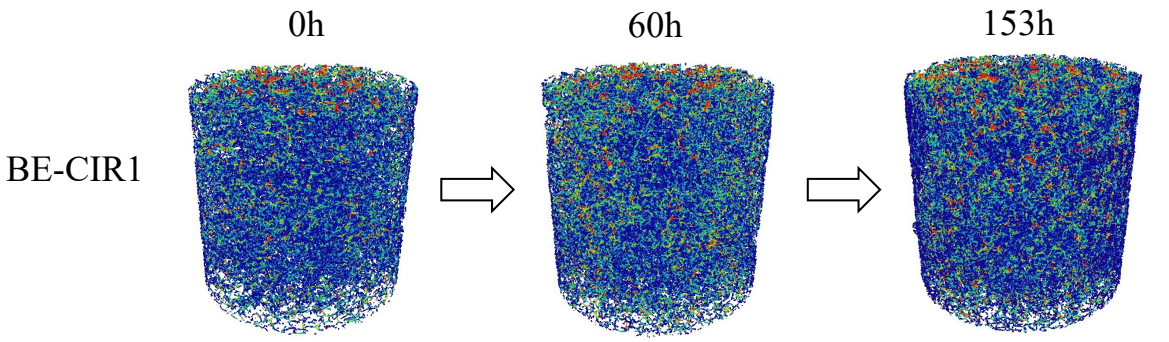

	0h	60h	153h
void number	57860	111873	187845
total volume(mm3)	36901	49193	57363

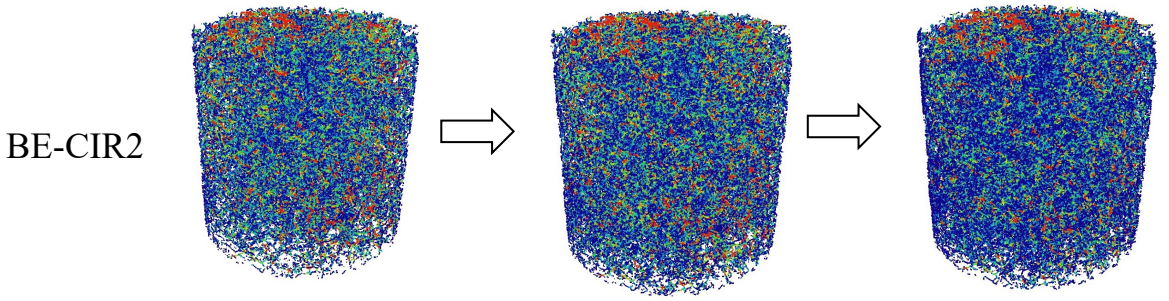

	0h	60h	153h
void number	106308	135846	220666
total volume(mm3)	48645.5	52847.9	54257.7

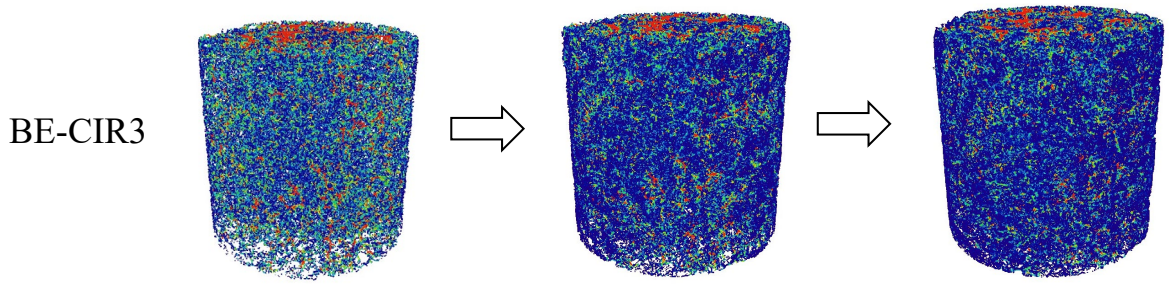

	0h	60h	153h
void number	103763	264968	408751
total volume(mm3)	41147.7	47856.2	59823.7

Figure 8 3D reconstruction of void and total void number and volume over curing time

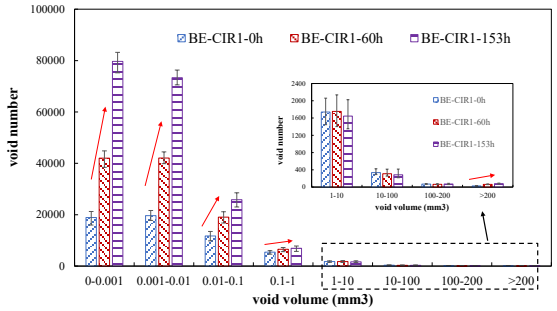

(a) Void number distribution of BE-CIR1

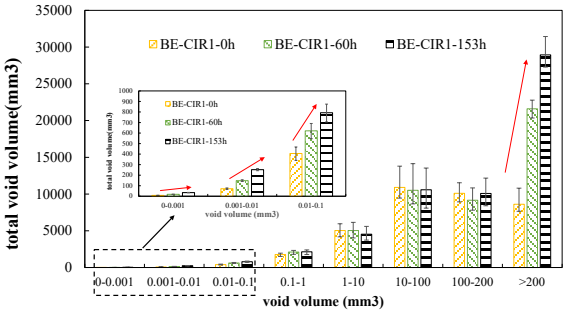

(b) Total void volume distribution of BE-CIR1

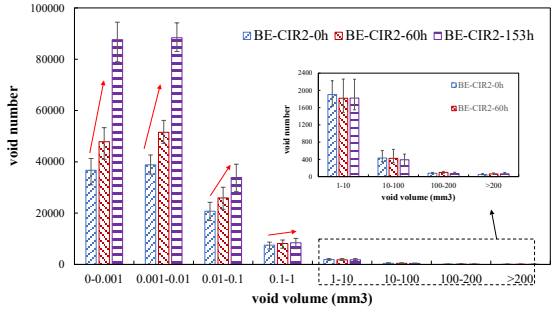

(c) Void number distribution of BE-CIR2

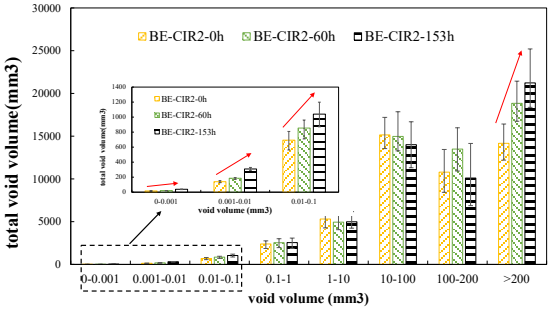

(d) Total void volume distribution of BE-CIR2

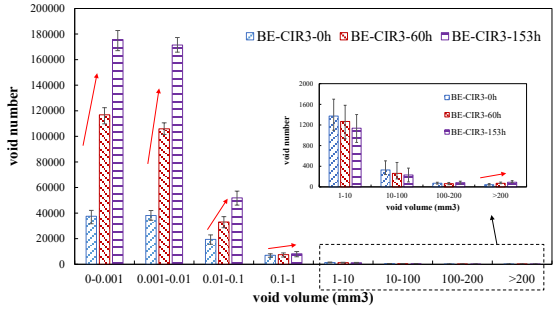

(e) Void number distribution of BE-CIR3

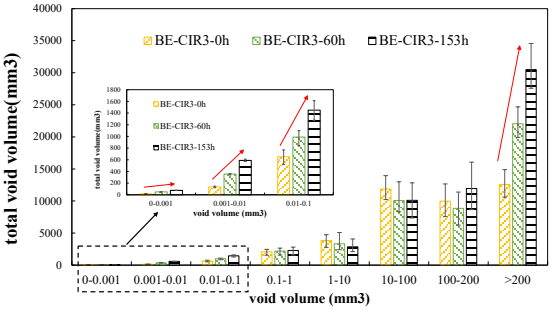

(f) Total void volume distribution of BE-CIR3

Figure 9 Distribution of voids number and volume

5.3.2 Total void volume distribution

Figure 8 3D reconstruction of void and total void number and volume over curing time

also shows the total void volume of each BE-CIR at different curing time. The total void volume of three BE-CIRs increased with curing time, but in different increase rate. Similar with the air void content, the volume increment of BE-CIR1 was greater than that of BE-CIR3 between 0 and 60 h, while BE-CIR3 was greater between 60 and 153h. The change in total void volume of BE-CIR2 is relatively small according to the same reason of air void content.

The sum of void volumes for each volume interval was calculated for three BE-CIRs at different curing time as illustrated in Figure 9 (b)(d)(f). Contrary to the distribution of numbers of voids for different volumes, although the number of voids in large volume is small, its contribution to the overall air void content is great. Same as the void number, the total void volume increased with curing time only in voids with the volume less than 1 mm^3 and bigger than 200 mm^3. From Figure 9, at curing time of 0h, the total volume of the three volume intervals with the greater volume (10-100 mm3, 100-200 mm^3, >200mm^3) were close. However, the total volume of voids larger than 200mm3 increased with the duration of curing time, while the other two intervals remained basically unchanged. This indicates that large voids were developing into more larger ones during the process of curing. Combined with the changes in the void number, it can be inferred that the development of medium-sized void is not significant, and voids with smaller volume appear rapidly.

5.4 Development of void gradation

The results of the void gradation for different BE-CIRs are presented in Figure 10. Since the gradation curves are relatively similar, in order to show the variation of void gradation over curing time, the difference in passing percentage for each sieve size at different curing time is defined as Δpassing percentage. Δpassing percentage is calculated by subtracting the value of shorter curing time from that of the longer curing time, i.e. Δpassing percentage for 0-60h is calculated by subtracting 0h from the corresponding passing percentage for 60h. Therefore, a negative Δpassing percentage suggests that the passing percentage at this sieve size becomes smaller during this curing period, which means that the volume of voids with a diameter larger than this size becomes larger. The variation in the void gradation for all CIR with increasing curing time showed a decrease in the passing percentage of larger sieve size and an increase in that of smaller size. The Δpassing percentage varied from greater than 0 to less than 0 as the sieve size increases, and the change occurred essentially between size of 0.6 mm and 1.18 mm. In other words, for all CIRs, the passing percentage increased with increasing curing time for sieve sizes smaller than 0.6 mm. In addition, the maximum of the absolute value of Δpassing percentage at all time periods was observed at the 6.7 mm sieve. This is consistent with the results of the void distribution analysis,

implying that pores with equivalent diameters less than 0.6 mm and greater than 6.7 mm increase continuously with curing.

For BE-CIR1, the Δpassing percentage at 0-60h was significantly greater than that at 60-153h, mainly when the sieve size was greater than 4.75 mm. While for BE-CIR2, the Δpassing percentage at 60-153h was greater than that at 0-60h and remains >0 at 60-153h when the pore size is ≤ 2.36. It can be inferred that the higher initial moisture content could lead to a smaller increase in small pores from 0-60h. This is mainly due to the fact that with a higher initial moisture content, water will gather on the surface of the specimen and evaporation of excessive water dominates in the early stages of curing, therefore the internal moisture changes to a lesser extent resulting in smaller void gradation change. The variation of void gradation in BE-CIR3 was similar to that of BE-CIR1, while the Δpassing percentage from 0-60h was significantly larger when the sieve size was small. The difference between 0-60h and 60-153h was also not as large as for BE-CIR1 of larger sieve size, suggesting that the magnitude of void development from 0-60h decreases significantly when the curing temperature is lower, which is consistent with the change in air void content.

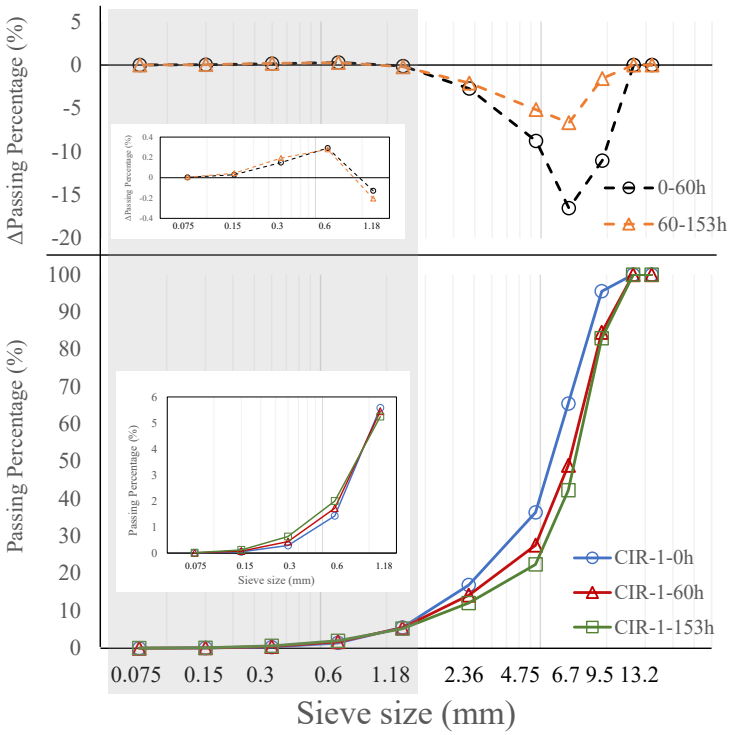

(a) Void gradation of BE-CIR1

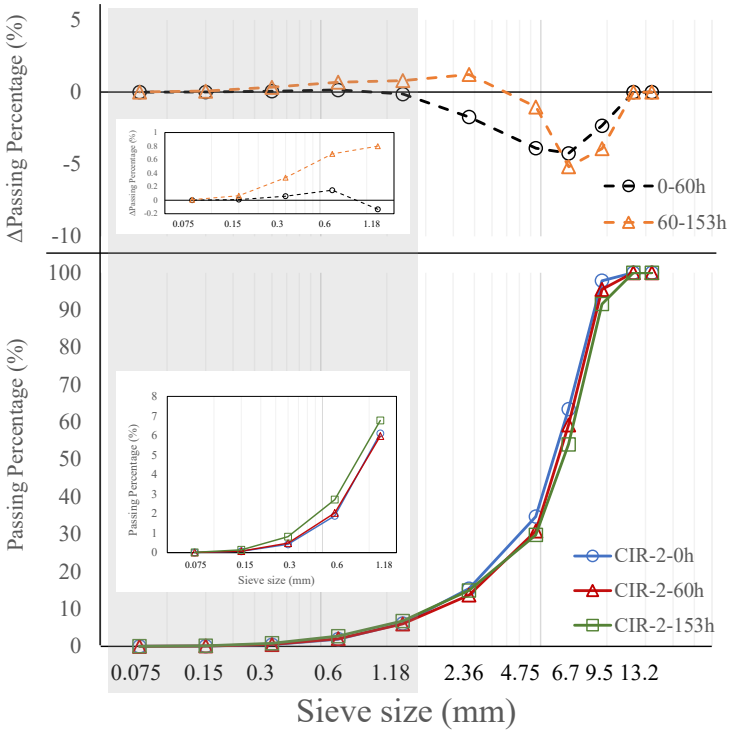

(b) Void gradation of BE-CIR2

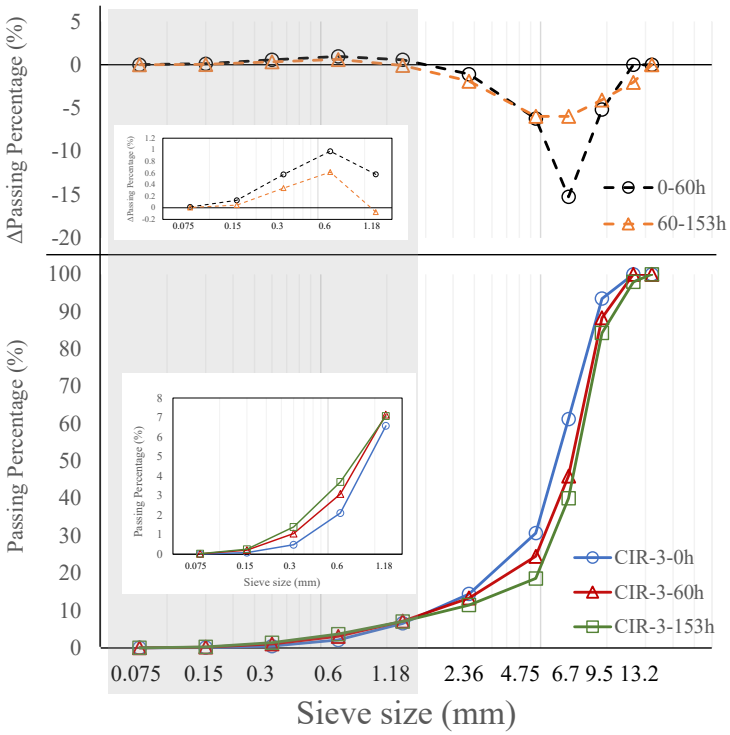

(c) Void gradation of BE-CIR3

Figure 10 Void gradation of different BE-CIRs

5.5 Distribution of voids in the depth direction

According to three-dimensional microstructures built every 10mm in the depth direction, the air void content of each region and the characters of each void could be obtained. The variation of each parameter in the direction of thickness was calculated by making the difference of results under different curing time, so as to analyze the development of air void of BE-CIR. In the analysis in this section, depth of 0-10mm represents the region closest to the upper surface of the specimen i.e. the side without waterproofing.

5.5.1 Air void content variation

The variation of air void content is defined as ΔAV, which is calculated by the air void content at different curing time. The distribution of ΔAV in the depth direction of three BE-CIR specimens at 0-60h and 60-153h as shown in Figure 11. During curing time of 0h to 60h, the ΔAV of BE-CIR1 and BE-CIR3 keep basically the same in the depth direction, while the ΔAV of BE-CIR2 during 0-60h decreased with depth increase, that is, the air void content in the region closer to the upper surface increased the most. Meanwhile, in the interval of curing time of 60 to153h, three CIRs all show the gradient characteristic of ΔAV in the depth direction, which means the smaller the depth, the greater the ΔAV. The gradient characteristics of BE-CIR1 and BE-CIR2 were more significant than BE-CIR3, which means the difference between ΔAV in the upper and lower regions is larger.

Theoretically, the variation of air void content during the curing of BE-CIR is mainly caused by internal moisture evaporation. And in this paper, moisture evaporation is only allowed from the upper surface (depth 0-10mm). From the comparison of ΔAV in the depth direction of three BE-CIRs, it can be inferred that CIR with higher initial water content has a faster moisture evaporation rate in the region closer to the upper surface at the beginning of the regimen (0-60h). In the later period of curing (60-153h), the influence of temperature on water evaporation was more significant, leading to the CIR with higher curing temperature exhibited obvious water evaporation gradient. In addition, only BE-CIR3 showed a significant feature of ΔAV was large at upper and bottom regions while small in middle region, which may be caused by its low curing temperature. When the curing temperature is low, the water evaporates slowly, and the water migrates slowly from

bottom to the upper region. Therefore, some moisture may be deposited at the bottom, resulting in large ΔAV in the bottom region. Finally, the difference in air void content between the top and bottom is approximately 0.5% at curing time of 153h for all three BE-CIRs.

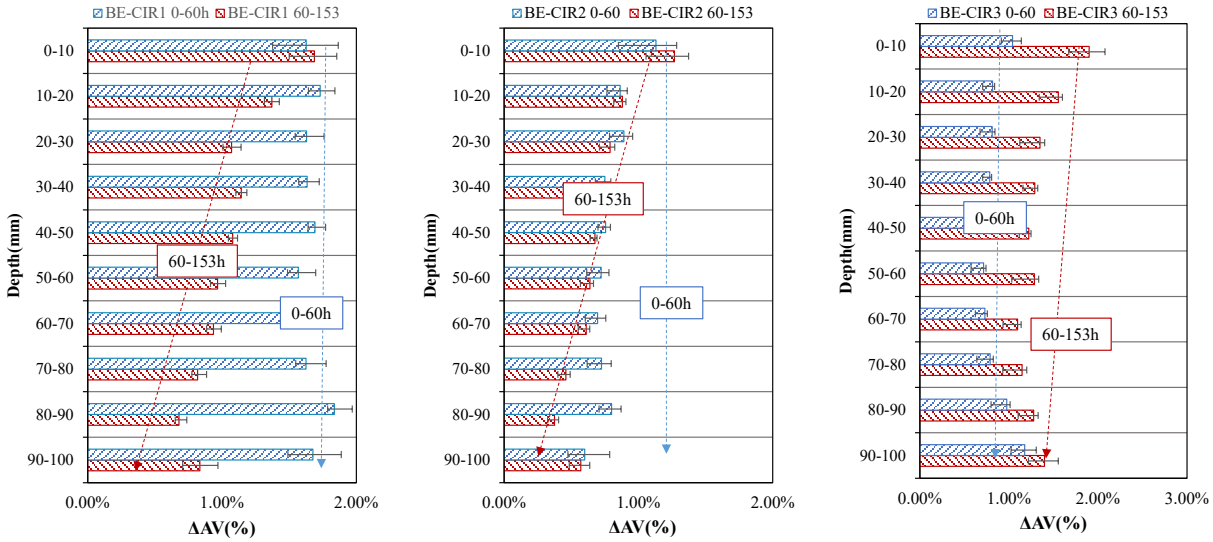

(a) BE-CIR1 (b) BE-CIR2 (c) BE-CIR3

Figure 11 Variation of air void content with curing time (ΔAV) in the depth direction

5.5.2 Void number variation

The difference of void number at different curing time is defined as ΔVN. From section 5.3.1 it was found that the void number increases with curing time, thus ΔVN refers to increment of the void number at different times. Figure 12 illustrates the distribution of ΔVN in the depth direction of three BE-CIR specimens at 0-60h and 60-153h. The increase in void number is observed to be heterogeneous in the depth direction of the specimen, with ΔVN essentially increasing the closer the region is to the surface. It is known that the increase in void number is almost attributed to the internal migration of moisture. The gradient distribution of ΔVN proves that the water migrated from the bottom to the top of the specimen during curing time, as this paper restricts the evaporation of water only from the surface.

Comparing the variation of ΔVN for the different BE-CIRs in 0-60h and 60-153h, only the ΔVN of BE-CIR2 in 0-60h is special, which does not show a clear gradient distribution characteristic in the depth direction. It is probable that due to the higher initial moisture content of BE-CIR2, there

is more extra moisture on the surface of the specimen at the very beginning of the curing, with free water near the surface evaporating first and internal moisture migration not being significant at this stage.

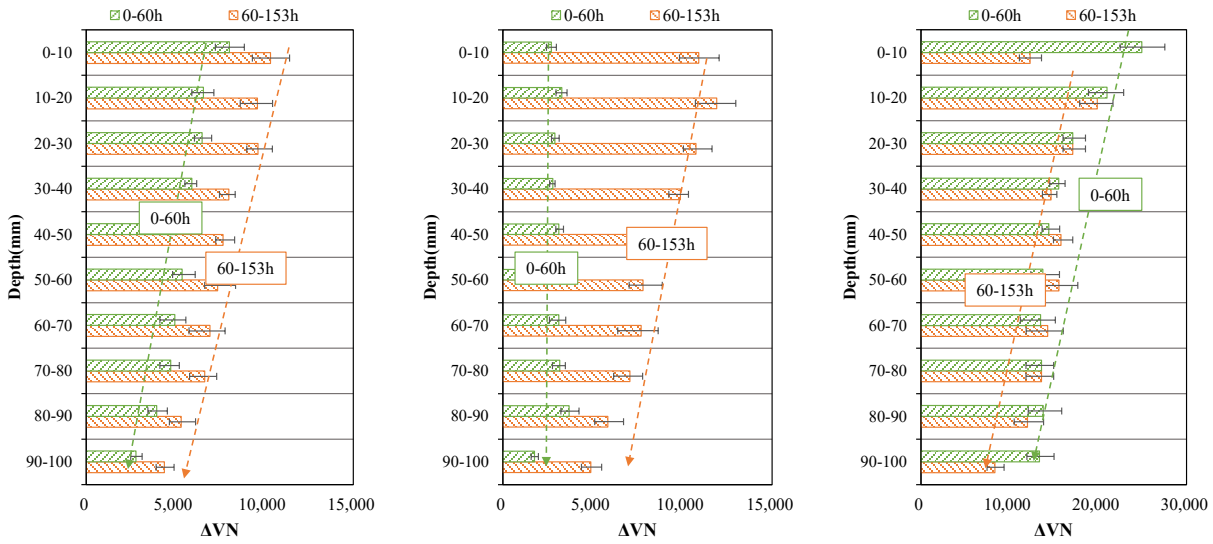

(a) BE-CIR1 (b) BE-CIR2 (c) BE-CIR3

Figure 12 Distribution of void number variation(ΔVN) in the depth direction

5.5.3 Variation of void with different volumes

According to section 5.4, voids with a volume of less than 0.1 mm^3 made up the majority of the void number distribution, while voids with a volume greater than 0.1 mm^3 accounted for the majority of the void volume distribution, so separate statistical analysis is required for the voids with different volumes. ΔVV is defined as the total volume change of pores during different curing time. Figure 13 shows the results of ΔVV and ΔVN for voids with volume less than 0.1 mm^3 and greater than 0.1 mm^3. The graph reveals that voids volume <0.1 mm^3 displayed a gradient distribution in the depth direction for both ΔVV and ΔVN, namely the closer to the sample surface (the smaller the depth), the larger the corresponding index. However, for voids > 0.1 mm^3 there is no uniform pattern in the depth direction for either the number or the volume variation. Meanwhile, there are also negative values of ΔVN for void volumes >0.1 mm^3, suggesting that there is also a degree of reduction in the number of larger volumes of voids as the curing time increases, which may be due to the merging of voids. This phenomenon demonstrates that the pore development of

the BE-CIR mixture during the curing is dominated by an increase in small pores, and that the closer the area to the surface, the greater the increase in void with smaller volume as a result of the process of moisture migration.

In addition, comparing the magnitudes of ΔVV and ΔVN for curing time of 0-60h and 60-153h, it is evident that for void volumes <0.1 mm^3, ΔVV and ΔVN during 60-153h were essentially greater than that in 0-60h for all of three BE-CIRs. When the void volume is >0.1 mm^3, the ΔVV and ΔVN during 60-153h were smaller for BE-CIR1 and BE-CIR2, while for BE-CIR3, the ΔVV and ΔVN during 60-153h were larger. This would suggest when the curing temperature is high, in the early stages of curing(0-60h), the flowable free water within the mix flows and evaporates rapidly at this stage, manifesting as an increase in the volume and possibly the number of larger voids. Once the regeneration temperature decreases, the rapid flow and evaporation of moisture slows down and the increase in the volume of larger pores is more significant in 60-153h. In addition, the effect of initial moisture content is mainly reflected in the effect on the initial migration of water within the mix, and there is no gradient characteristic of pore volume change along the depth direction within the mix from 0-60h.

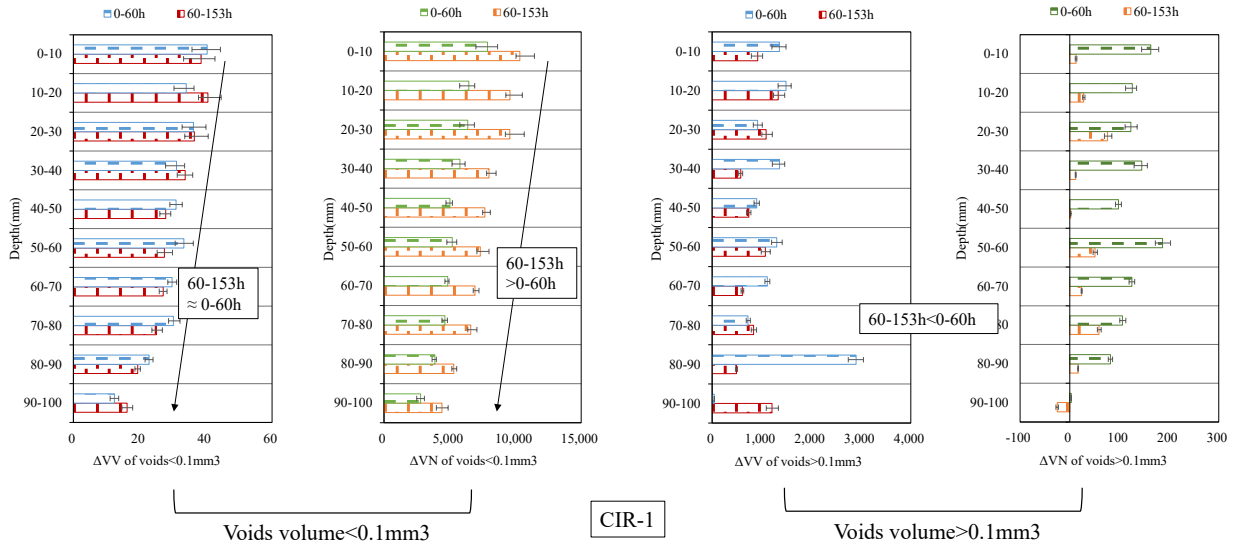

(a) BE-CIR1

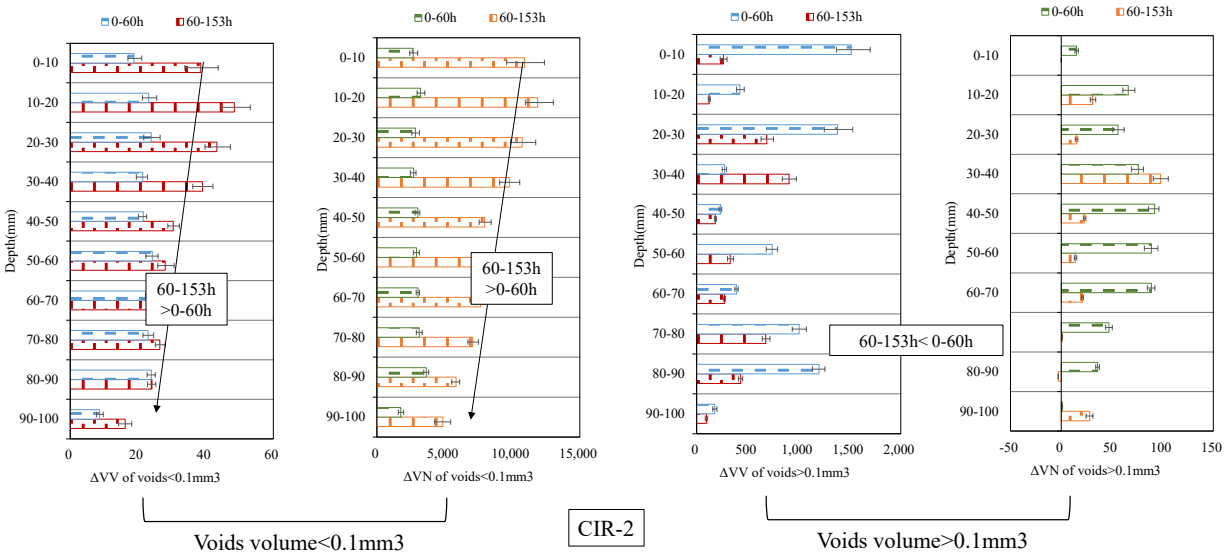

(b) BE-CIR2

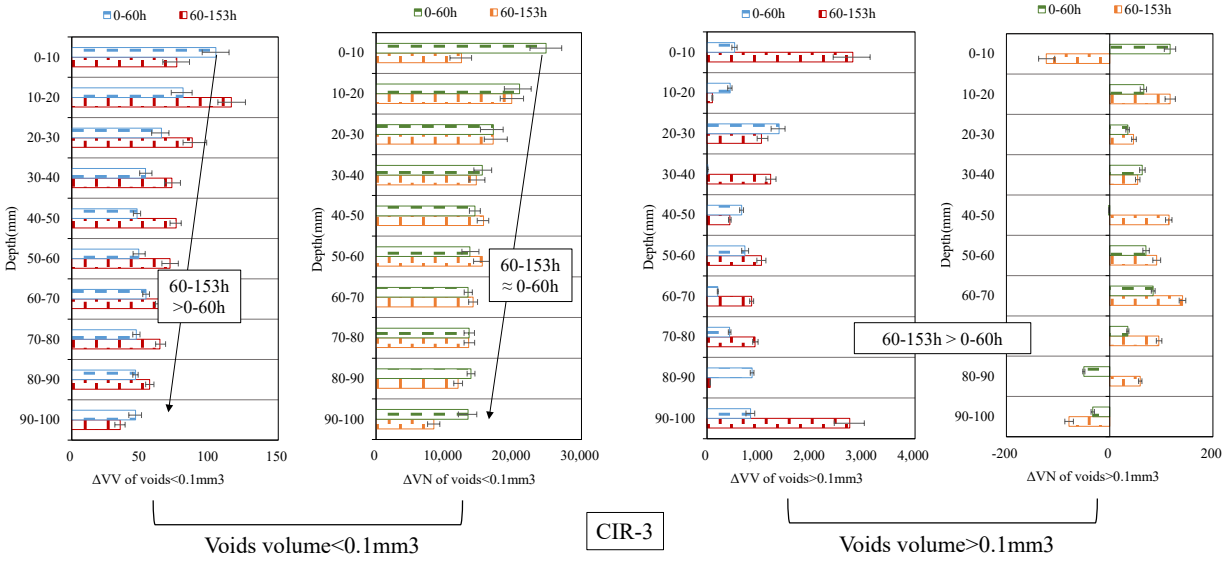

(c) BE-CIR3

Figure 13 Void number variation(ΔVN) and total volume variation (ΔVV) for voids with different volumes in the depth direction

6 Conclusions

In this study, CT scanning tests were conducted to investigate the micropore development of BE-CIR mixes during the curing process. A curing method simulating the field moisture migration was setup in the laboratory. The three-dimensional reconstruction was conducted on both the whole specimen and sub-regions in the depth direction to analyze the patterns of change in void

structure due to water migration during curing. Meanwhile, the effects of both curing temperature and initial moisture content were considered. The main conclusions can be drawn as follows:

(1) During curing process, the weight loss of BE-CIR mixture increases rapidly and then becomes stable. Air void content increases with curing time because of the water evaporation. Lower curing temperature significantly reduces the weight loss rate and air void generation in the first 60 hours of curing. More additional water may contribute to not only the coating of bitumen emulsion but also a greater void content in mineral aggregates.

(2) The micropore structure of BE-CIR mixture evolves over the course of curing with two typical characteristics, namely the fast increase in the number of small voids and the sustained development of large voids. For our case, the first stage of curing (0 to 60hours) exhibited more significant variation of larger pores, while the second stage of curing (60 to 153hours) manifested as a greater increase of small pores indicating the different form of water migration.

(3) The variation of air void content and the void number in the depth direction of the specimen have gradient characteristics of more near the surface and less at the bottom after curing. The gradient distribution was mainly manifested in the number and volume variation of voids with volume smaller than 0.1 mm3, and it was mainly formed during the second curing stage. The difference in air void content between the top and bottom could be 0.5% after curing.

(4) Higher initial moisture content may result in a significant decrease in the generation of micropores smaller than 1 mm3 at curing time of 0 to 60hours, and a less pronounced gradient distribution in the depth direction. Higher curing temperature enlarges the proportion of air void generation between the two curing periods and contributes to a more significant gradient distribution.

To sum up, there are significant differences in the microstructure of the upper and lower parts of the mix after regeneration. Since the water in the upper part evaporates more easily, leading to more small pores and a larger air void content. This may contribute to great influence on the mechanical behavior of BE-CIR, and this will be investigated in the future studies. Moreover, it is necessary to further go to the nano pore development with the help of more advanced testing methods, which can shed more lights on the microstructural formation of the BE-CIR mixtures.

Acknowledgement

The data used in this study was collected from a maintenance project in Fenguan highway and supported by the Jiangsu Communications Holding Co.,Ltd. This work was also supported by the National Natural Science Foundation of China (Grant No. 52108421), the Hong Kong Research Grant Council through the GRF project (Grant No. 15220621) and the Fundamental Research Funds for the Central Universities (Grant No. 3221002139D).

References

[1] F. Gu, W.Y. Ma, R.C. West, A.J. Taylor, Y.Q. Zhang, Structural performance and sustainability assessment of cold central-plant and in-place recycled asphalt pavements: A case study, Journal of Cleaner Production 208 (2019) 1513-1523.
[2] A. Modarres, M. Rahimzadeh, M. Zarrabi, Field investigation of pavement rehabilitation utilizing cold in-place recycling, Resources Conservation and Recycling 83 (2014) 112-120.
[3] J. Turk, A.M. Pranjic, A. Mladenovic, Z. Cotic, P. Jurjavcic, Environmental comparison of two alternative road pavement rehabilitation techniques: cold-in-place-recycling versus traditional reconstruction, JOURNAL OF CLEANER PRODUCTION 121 (2016) 45-55.
[4] A.E. Alkins, B. Lane, T. Kazmierowski, Sustainable Pavements Environmental, Economic, and Social Benefits of In Situ Pavement Recycling, TRANSPORTATION RESEARCH RECORD (2084) (2008) 100-103.
[5] F. Xiao, S. Yao, J. Wang, X. Li, S. Amirkhanian, A literature review on cold recycling technology of asphalt pavement, Construction and Building Materials 180 (2018) 579-604.
[6] L.N. Mohammad, M.Y. Abu-Farsakh, Z. Wu, C. Abadie, Trb, Trb, Louisiana experience with foamed recycled asphalt pavement base materials, Bituminous Paving Mixtures 2003: Materials and Construction2003, pp. 17-24.
[7] K. Kuna, G. Airey, N. Thom, Mix design considerations of foamed bitumen mixtures with reclaimed asphalt pavement material, International Journal of Pavement Engineering 18(10) (2017) 902-915.
[8] Z.L. Zhao, J.W. Jiang, Z.W. Chen, F.J. Ni, Moisture migration of bitumen emulsion-based cold in-place recycling pavement after compaction: Real-time field measurement and laboratory investigation, Journal of Cleaner Production 360 (2022).
[9] X. Zhao, Research on Application of Cold In-place Recycled Technology with Modified Emulsified Asphalt in Middle Surface Layer of Highway, Southeast university, 2020.
[10] A. Grilli, A. Graziani, E. Bocci, M. Bocci, Volumetric properties and influence of water content on the compactability of cold recycled mixtures, Materials and Structures 49(10) (2016) 4349-4362.
[11] S.W. Du, The Optimum Pre-mixing Water Content in Asphalt Emulsion Mixture with Cement, Journal of Testing and Evaluation 49(6) (2021) 4560-4575.
[12] A. Graziani, C. Godenzoni, F. Cardone, M. Bocci, Effect of curing on the physical and mechanical properties of cold-recycled bituminous mixtures, Materials & Design 95 (2016) 358-369.
[13] P. Orosa, I. Pérez, A.R. Pasandín, Short-term resilient behaviour and its evolution with curing in cold in-place recycled asphalt mixtures, Construction and Building Materials 323 (2022) 126559.
[14] W.T. Yang, J. Ouyang, Y. Meng, B.G. Han, Y.Q. Sha, Effect of curing and compaction on volumetric and mechanical properties of cold-recycled mixture with asphalt emulsion under different cement contents, Construction and Building Materials 297 (2021).
[15] M. Golian, H. Katibeh, V.P. Singh, K. Ostad-Ali-Askari, H.T. Rostami, Prediction of tunnelling impact on flow rates of adjacent extraction water wells, Quarterly Journal of Engineering Geology and Hydrogeology 53
(2) (2020) 236-251.
[16] Y.H. Yang, H.B. Wang, Y. Yang, H.Z. Zhang, Evaluation of the evolution of the structure of cold recycled mixture subjected to wheel tracking using digital image processing, Construction and Building Materials 304 (2021).
[17] F. Cardone, A. Grilli, M. Bocci, A. Graziani, Curing and temperature sensitivity of cement-bitumen treated materials, International Journal of Pavement Engineering 16(10) (2015) 868-880.
[18] A. Graziani, C. Iafelice, S. Raschia, D. Perraton, A. Carter, A procedure for characterizing the curing process of cold recycled bitumen emulsion mixtures, Construction and Building Materials 173 (2018) 754-762.
[19] P.C. Fu, D. Jones, J.T. Harvey, F.A. Halles, Investigation of the Curing Mechanism of Foamed Asphalt Mixes Based on Micromechanics Principles, Journal of Materials in Civil Engineering 22(1) (2010) 29-38.

[20] M. Pasetto, E. Pasquini, A. Baliello, S. Raschia, A. Rahmanbeiki, A. Carter, D. Perraton, F. Preti, B.C.S. Gouveia, G. Tebaldi, Influence of curing on the mechanical properties of cement-bitumen treated materials using foamed bitumen: An interlaboratory test program, Proceedings of the 9th International Conference on Maintenance and Rehabilitation of Pavements—Mairepav9, Springer, 2020, pp. 55-65.
[21] C. Raab, M.N.J.A.i.M.S. Partl, Engineering, Laboratory evaluation and construction of fully recycled low-temperature asphalt for low-volume roads, 2020 (2020).
[22] K. Jenkins, C. Rudman, C.J.A.i.M.S. Bierman, Engineering, Delivering sustainable solutions through improved mix and structural design functions for bitumen stabilised materials, 2020 (2020).
[23] A. Graziani, A. Grilli, C. Mignini, A. Balzi, Assessing the Field Curing Behavior of Cold Recycled Asphalt Mixtures, Advances in Materials Science and Engineering 2022 (2022).
[24] P. Orosa, G. Orozco, J. Carret, A. Carter, I. Pérez, A.J.C. Pasandín, B. Materials, Compactability and mechanical properties of cold recycled mixes prepared with different nominal maximum sizes of RAP, 339 (2022) 127689.
[25] A. Woods, Y. Kim, H. Lee, Determining Timing of Overlay on Cold In-Place Recycling Layer Development of New Tool Based on Moisture Loss Index and In Situ Stiffness, Transportation Research Record (2306) (2012) 52-61.
[26] B.C. Cox, I.L. Howard, Cold in-place recycling characterization framework and design guidance for single or multiple component binder systems, 2015.
[27] B.C. Cox, I.L. Howard, C.S. Campbell, Cold In-Place Recycling Moisture-Related Design and Construction Considerations for Single or Multiple Component Binder Systems, Transportation Research Record (2575) (2016) 27-38.
[28] L. Gao, F.J. Ni, C. Ling, J.H. Yan, Evaluation of fatigue behavior in cold recycled mixture using digital image correlation method, Construction and Building Materials 102 (2016) 393-402.
[29] E. Masad, V. Jandhyala, N. Dasgupta, N. Somadevan, N.J.J.o.m.i.c.e. Shashidhar, Characterization of air void distribution in asphalt mixes using X-ray computed tomography, 14(2) (2002) 122-129.
[30] X. Lu, P. Redelius, H. Soenen, M.J.R.m. Thau, p. design, Material characteristics of long lasting asphalt pavements, 12(3) (2011) 567-585.
[31] L. Gao, F. Ni, H. Luo, S. Charmot, Characterization of air voids in cold in-place recycling mixtures using X-ray computed tomography, Construction and Building Materials 84 (2015) 429-436.
[32] M.K. Nivedya, A. Veeraragavan, P. Ravindran, J.M. Krishnan, Investigation on the Influence of Air Voids and Active Filler on the Mechanical Response of Bitumen Stabilized Material, Journal of Materials in Civil Engineering 30(3) (2018).
[33] MOT, JTG E20-2011, Standard Test Methods of Bitumen and Bituminous Mixtures for Highway Engineering (in Chinese), 2011.
[34] J.P. DOT, Applied Manual for Asphalt Emulsion Cold In-Place Recycling Technology, China, 2010.